JACS
JOURNAL OF THE AMERICAN CHEMICAL SOCIETY

Article

pubs.acs.org/JACS

Millifluidics for Time-resolved Mapping of the Growth of Gold Nanostructures

Katla Sai Krishna,[†,∥] Chelliah V. Navin,[†,‡] Sanchita Biswas,[†] Varshni Singh,[†] Kyungmin Ham,[†] G. Lisa Bovenkamp,[†] Chandra S. Theegala,[‡] Jeffery T. Miller,[§] James J. Spivey,[∥] and Challa S. S. R. Kumar*[,†,∥]

[†]Center for Advanced Microstructures and Devices (CAMD), Louisiana State University, Baton Rouge, Louisiana 70806, United States

[‡]Department of Biological and Agricultural Engineering, and LSU AgCenter, Louisiana State University, Baton Rouge, Louisiana 70803, United States

[§]Argonne National Laboratory, 9700 South Cass Avenue, CSE, Argonne, Illinois 60439-4837, United States

[∥]Center for Atomic-Level Catalyst Design, #324, Cain Department of Chemical Engineering, Louisiana State University, Baton Rouge, Louisiana 70803, United States

Supporting Information

ABSTRACT: Innovative *in situ* characterization tools are essential for understanding the reaction mechanisms leading to the growth of nanoscale materials. Though techniques, such as *in situ* transmission X-ray microscopy, fast single-particle spectroscopy, small-angle X-ray scattering, etc., are currently being developed, these tools are complex, not easily accessible, and do not necessarily provide the temporal resolution required to follow the formation of nanomaterials in real time. Here, we demonstrate for the first time the utility of a simple millifluidic chip for an *in situ* real time analysis of morphology and dimension-controlled growth of gold nano- and microstructures with a time resolution of 5 ms. The structures formed were characterized using synchrotron radiation-based *in situ* X-ray absorption spectroscopy, 3-D X-ray tomography, and high-resolution electron microscopy. These gold nanostructures were found to be catalytically active for conversion of 4-nitrophenol into 4-aminophenol, providing an example of the potential opportunities for time-resolved analysis of catalytic reactions. While the investigations reported here are focused on gold nanostructures, the technique can be applied to analyze the time-resolved growth of other types of nanostructured metals and metal oxides. With the ability to probe at least a 10-fold higher concentrations, in comparison with traditional microfluidics, the tool has potential to revolutionize a broad range of fields from catalysis, molecular analysis, biodefense, and molecular biology.

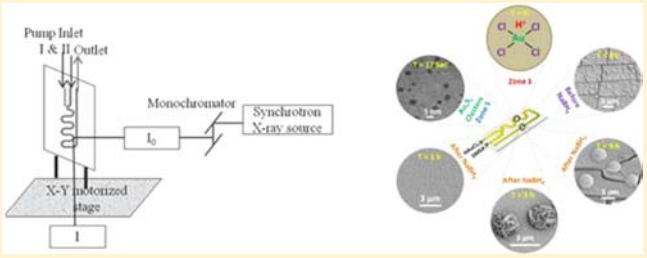

INTRODUCTION

A number of synchrotron radiation-based X-ray characterization tools[1,2] are used for both chemical and physical characterization of materials, especially in a liquid environment. Among these, X-ray absorption spectroscopy (XAS) is a versatile tool to probe oxidation states, coordination, and local order of materials, even in the absence of a crystalline lattice. XAS has been used to investigate the electronic and geometric structures of nanomaterials; more specifically, to map local coordination number, the extent of alloying and composition of multimetallic systems in solution.[3] Further, *in situ* XAS offers an opportunity to observe time-resolved bond formation, changes in oxidation states, coordination, and local order.[4] The ability to follow the fundamental processes in the synthesis of nanostructured materials with atomic precision is an unfulfilled need in the field of nanoscience.

Microfluidic systems have been used to prepare a wide range of materials. These systems consist of small channels of micrometer dimensions in which the reactive liquid precursors needed to produce solid clusters of metals are mixed and allowed to react. Recently, they have become an attractive technology due to their ability to rapidly mix reagents, provide homogeneous reaction environments, continuously vary reaction conditions, add reagents at precise time intervals during reaction, and the ability to control the residence time by varying the reactant flow-rates and/or the length of the flow channel.[5−7] These features have been cleverly utilized in the wet-chemical synthesis of nanomaterials not only to control their size, size-distribution, and shape[8] but also to control their crystal structure[9] and for faster clinical translation.[10]

The use of XAS in conjunction with microfluidic systems provides a powerful new method for *in situ* time-resolved experiments probing the structure and reaction dynamics at

Received: January 14, 2013
Published: March 15, 2013

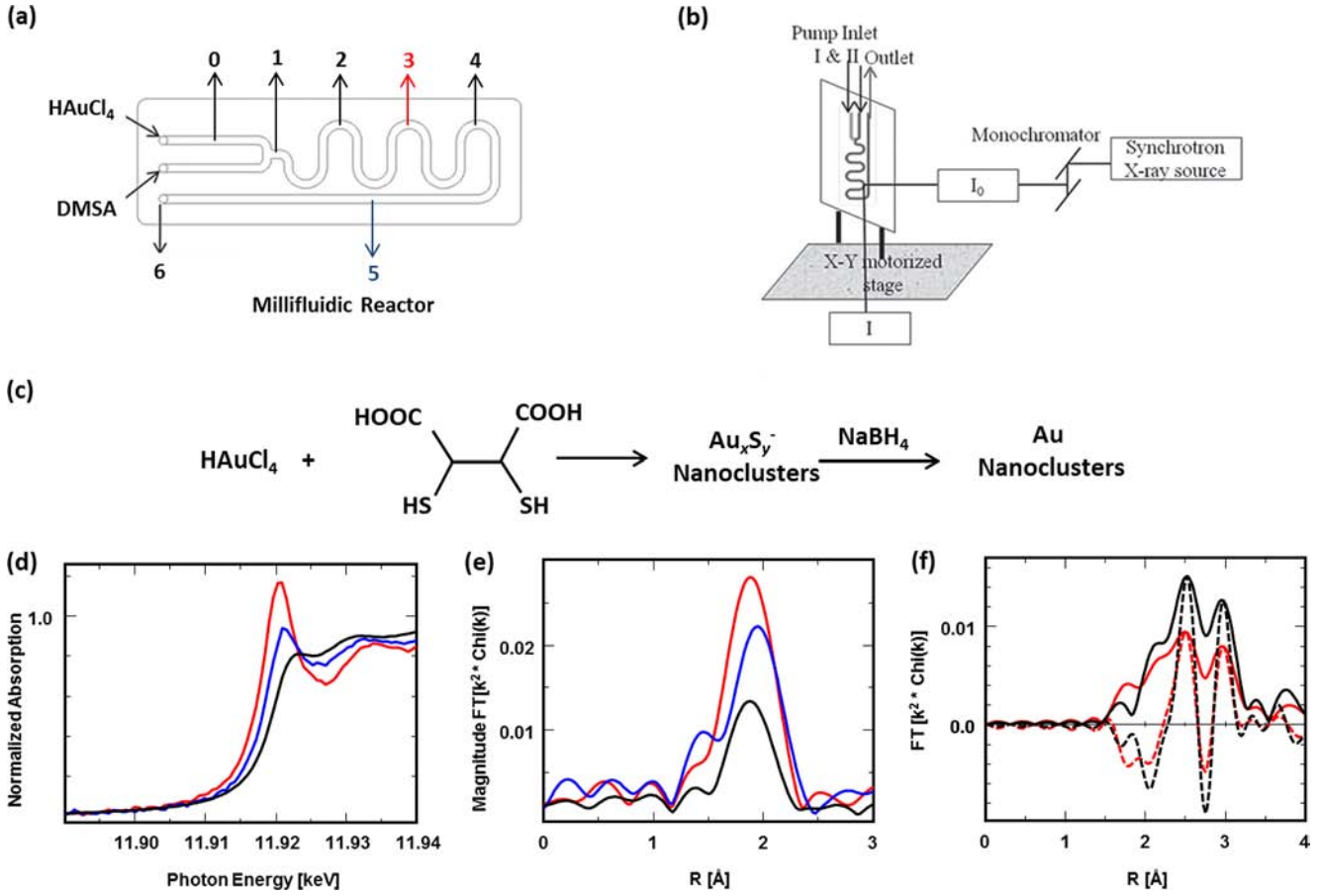

Figure 1. (a) Millifluidic chip marked with different zones where *in situ* XAS was performed. (b) In-situ XAS analysis at different zones within the millifluidic channel. (c) Reaction scheme of precursors. (d) XANES spectra showing the Au L_3-edge at zones 3 (red), 5 (blue) and at zone 5 after 12 h (black). (e) EXAFS spectra at the same zones. (f) EXAFS of Au foil (black) and sample after NaBH4 reduction (red); (—) Fourier transform magnitude and (- - -) imaginary component of the Fourier transform.

atomic level.[11] However, requirement for a sample concentration in excess of 0.1 M to obtain high-quality data has been a major drawback in utilizing microfluidic chips for *in situ* XAS analysis.[7] We have recently introduced the concept of chip-based millifluidics, which are very different from tubular millifluidics,[12] and demonstrated their advantages over traditional microfluidics for higher throughput controlled synthesis of ultrasmall nanoclusters.[13,14] Continuing from these investigations, herein, we demonstrate a step-up advance in utilizing this technique, which is simple and easily accessible unlike traditional microfluidics, as a probe for mapping time-resolved growth of nanomaterials. We show for the first time an *in situ* XAS analysis, in real time, of morphology-controlled growth of gold nanostructures within a millifluidic chip reactor. The reaction sequence of gold nanostructure formation with time resolution has been mapped. The central theme of these novel investigations is the utility of millifluidics for mapping the time-resolved chemistry of the growth of metallic structures in general and catalysts in particular. We also show continuous flow catalytic activity of the as-formed gold nanostructures for reduction of 4-nitrophenol and ferricyanide. While microfluidics-based continuous flow catalysis of gold nanoparticles impregnated on alumina has been previously utilized for synthesis of polypyridine derivatives,[15] the ability to control the dimension, and morphology of the embedded gold nanostructured catalysts within continuous flow channels was never explored before. The results reported are anticipated to lead to superior continuous flow catalysis applications. With the possibility to embed atomically precise catalysts, these tools can revolutionize catalysis from the point of view of practical as well as fundamental investigations.[16−18] Such systems are also likely to lead to advances in the field of biosensing,[19] electrophoresis,[20] and enhanced optical detection.[21] Additionally, the flower-like gold morphology obtained through this formation process has applications in surface-enhanced Raman spectroscopy,[22] catalysis,[23] bioimaging,[24] and superhydrophobic coatings.[25]

■ RESULTS AND DISCUSSION

The millifluidic chip used in this study consists of serpentine channels with dimensions of 2 mm (W) × 0.15 mm (H) × 220 mm (L). Each chip had two inputs and a single output which connects them to a manifold (Figures 1 and S1). Fully automated syringe pumps were programmed to dispense the reagent solutions through the chip at required flow-rates through a computer controlled software. A hand-held millifluidic device purchased from Millifluidica, LLC (www.millifluidica.com) was also found to be useful for investigating these reactions.

After optimizing the flow conditions, the precursor reagents (chloroauric acid ($HAuCl_4$) and *meso*-2, 3-dimercapto succinic acid (DMSA)) were dispensed within the chip at a flow-rate of 10 mL/h and allowed to react at zone 1 (Figure 1a,c). At the flow-rates utilized, the Reynolds numbers are low (for example,

dx.doi.org/10.1021/ja400434c | J. Am. Chem. Soc. 2013, 135, 5450−5456

Table 1. Results of the *in Situ* Au EXAFS Analysis

sample	Au^{+3} ($HAuCl_4$)	Au^{+1} ($Au_xS_y^-$)	Au^0	edge energy, keV	scattering pair	N	R, Å	$\Delta\sigma^2$ ($\times 10^3$)	E_o, eV
$HAuCl_4$	1.0	–	–	11.9182	Au–Cl	4.0	2.28	0.0	−0.5
zone 3	1.0	–	–	11.9182	Au–Cl	4.2	2.27	0.0	−0.2
zone 4	1.0	–	–	11.9185	Au–Cl	4.0	2.29	0.0	1.5
zone 5	0.4	0.6	–	11.9189	Au–Cl(S)	3.0	2.29	0.0	−0.2
after 12 h	–	1.0	–	11.9195	Au–S	2.0	2.30	0.0	−2.9
$NaBH_4$	–	–	1.0	11.9191	Au–Au	8.7	2.86	1.0	−0.8
					Au–S	0.4	2.31	0.0	−4.1
Au foil	–	–	1.0	11.9190	Au–Au	12.0	2.88	0.0	0.0

2.57×10^{-4} at 1 mL/h). Under these conditions, the flow is completely laminar, and the two precursor solutions do not mix except at the interface. Rather, they remain as separate solution streams on either side of the rectangular cross-section, and the reaction between them occurs only at the interface of the two streams. It is at this interface that the gold nanostructures are formed, producing first a controlled deposit of solid gold sulfide at the bottom center of the channel that is later reduced to metallic gold by flowing $NaBH_4$ as a reducing agent through the entire channel. To understand the time-resolved chemical nature of the gold nanostructures formed, *in situ* XAS was carried out at different positions on the chip during the reaction. For this purpose, the chip was mounted onto a metal stage that could be adjusted in three dimensions. The mount was then placed in the path of the monochromatized synchrotron beam and adjusted such that the beam passed through the desired zone on the chip (Figure S2). Prior to the start of the reaction, the channel mapping at Au L_3-edge was carried out by dispensing only $HAuCl_4$ solution through the channels. The channel was marked for probing at five different zones (Figure 1a) and the XAS spectra were collected at each of the five zones, probed by an X-ray beam size of 0.05 × 0.05 mm, while flowing the precursor solutions into the channels (Figure 1b). The spectra from zones 1–4 were found to be exactly similar to that of $HAuCl_4$ solution. The first changes in the spectra were noticed at zone 5. After this initial study, zones 3 and 5 were chosen for more detailed analysis. Figure 1d shows the Au L_3-edge XANES spectra collected at zones 3 and 5 on the chip immediately after passing the precursors and at zone 5 after 12 h. The spectrum obtained at zone 3 matched well with that of the precursor, $HAuCl_4$, having Au(III) oxidation state (Table 1). The spectrum obtained at zone 5 showed a mixture of $HAuCl_4$ and also the formation of $Au_xS_y^-$ nanoclusters[26] having an Au/S ratio close to 2 with Au(I) oxidation state. The transmission electron microscopy (TEM) image of the sample collected from the same zone (by dissecting the chip at this location) also confirmed the formation of $Au_xS_y^-$ nanoclusters of 1–2 nm size (Figure S3). The EXAFS spectrum of the sample probed at zone 5 showed the presence of 40% of $HAuCl_4$ and 60% of the $Au_xS_y^-$ nanoclusters (Figure 1e, and Table 1) based on the linear combination fitting with gold foil and gold sulfide reference compounds. The formation of $Au_xS_y^-$ nanoclusters was observed 17 s after injecting the precursor solutions and the reaction rate (calculated based on the consumption of precursor) at this point was 0.235 $mmol^{-1}$. However, complete formation of the $Au_xS_y^-$ nanoclusters was observed only after 12 h duration (Figures 1d,e, and Table 1). Interestingly, the $Au_xS_y^-$ nanoclusters were stable even after 24 h, and there was no evidence of Au–Au bonding until the addition of $NaBH_4$. Tsukuda and co-workers[27] reported the formation of metallic $Au_{13}(DMSA)_8$ clusters with Au–Au bonding upon mixing of the same precursors in a traditional flask synthesis. Our *in situ* XAS results showed that the Au(III) (from the $HAuCl_4$) was converted to only Au(I) and not to Au(0) until the addition of $NaBH_4$. The matrix-assisted laser desorption ionization (MALDI) mass spectra of the nanoclusters prepared within a conventional flask under similar conditions showed formation of a mixture of ultrasmall $Au_n(SR)_m$ clusters with 10–13 gold atoms (Figure S4). After passing $NaBH_4$ through the chip, the bond length of the nanoclusters increased from 2.30 (Au–S) to 2.86 Å (Au–Au) indicating the reduction of Au(I) to Au(0) (Figure 1f). The generality of the technique, therefore, is that it provides an opportunity to observe the reaction intermediates at different zones with a spatial resolution corresponding directly to time resolution. This approach can be used to probe reactions in real-time to understand reaction kinetics and mechanism. For example, the products formed within the channel at a flow-rate of 10 mL/h can be analyzed with a time resolution of 5.4 ms (Figure S5). By increasing the flow-rate further, there is a potential opportunity to increase this time resolution from milliseconds to nanoseconds.[28]

The same millifluidics tool was also applied to study the growth of gold nanostructures, at a larger time interval, as they further grew into macroscopic structures. This was possible by monitoring the growth after 1, 5, and 9 h on line while keeping the flow-rate constant at 1 mL/h. During these three time periods, the morphology of the gold nanostructures changed dramatically. The morphology of the resultant gold structures formed at different flow-times were probed using scanning electron microscope (SEM). Figure 2 illustrates the SEM images of the gold structures formed at three different flow-times (1, 5, and 9 h respectively). Figure 2a shows the low magnification SEM image of the gold structures formed at 1 h flow-time. Randomly shaped polygonal nanoparticles of ∼300 nm (inset of Figure 2a) were observed at this stage. There were no structures observed at flow-times <1 h. When the flow-time was increased to 5 h, the gold structures formed appeared to have flower-like morphology as seen in Figure 2b. The structures were ∼3 μm in diameter and had corrugated petal-like nanostructured features. The figure inset of Figure 2b shows a magnified view of the same microflowers where one could clearly see a porous structure containing multiple grooves of sizes 100–200 nm. Figure 2c shows a low-magnification SEM image of the gold coating obtained at 9 h flow-time, where one could see further transformation of flower-like morphology into microspherical structures. A closer view of these structures (Inset of Figure 2c) showed the microstructures to be hemispherical in shape. The gold hemispheres were ∼3 μm in diameter and had a rough nanostructured porous surface, which was evident from the higher magnified images. The structures seem to be formed from the fusion of numerous

dx.doi.org/10.1021/ja400434c | J. Am. Chem. Soc. 2013, 135, 5450–5456

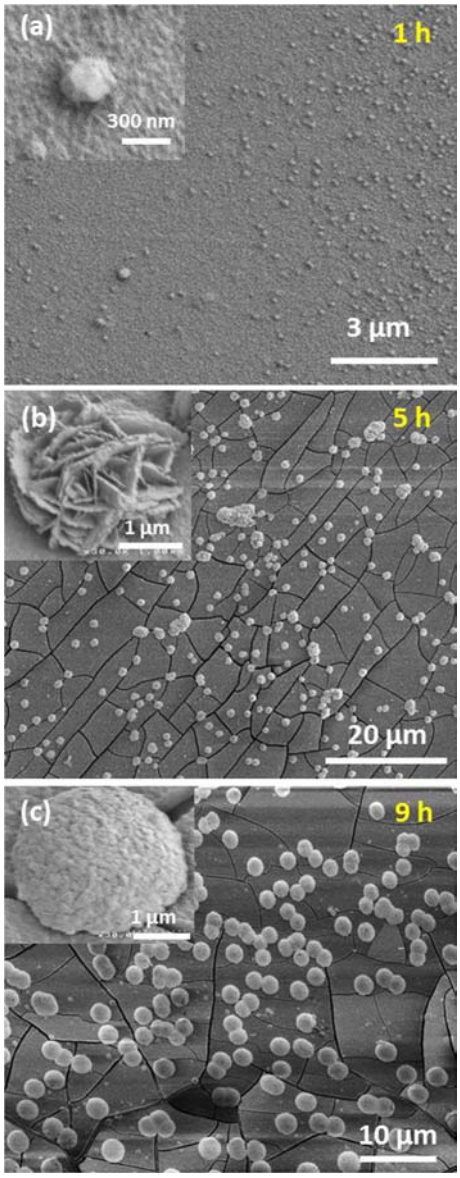

Figure 2. SEM images of the gold structures formed within the millifluidic channels with flow-times: (a) 1, (b) 5, and (c) 9 h. Insets show the magnified images of a single structure.

smaller-sized particles generating occasional pores on its curved surface. Such irregular rough surfaces are usually preferred for their high surface area and are commonly found in electrocatalysts.[29] Hemispherical shape was probably formed due to the lower surface area per given volume (in order to reduce surface energy) attributed to that shape. Formation of such gold hemispheres is rarely reported in the literature,[30] and this is the first report of their formation within a continuous flow chip.

The structures formed at intermediate flow-times, such as 3 and 7 h, were also analyzed. However, they showed incompletely formed flowers and hemispheres (Figure S6). The SEM image of $Au_xS_y^-$ structures formed at 9 h flow-time without the $NaBH_4$ reduction also showed formation of similar hemispherical structures indicating the retention of similar morphologies before and after reduction (Figure S7). While these morphology changes with flow-time were observed at constant flow-rate, we have also investigated the influence of increasing flow-rate. When the flow-rate was increased to 12 mL/h, formation of an increased number of even smaller spherical structures was noticed more quickly; just after 45 min (Figure S8). It is clear that the gold structures appear to evolve with time depending on the flow-rate as well as flow-times.

A schematic summarizing the time-resolved mapping of the growth of gold nanostructures within the millifluidic chip is given in Figure 3. As seen from the Figure 3a, zone 3 is a

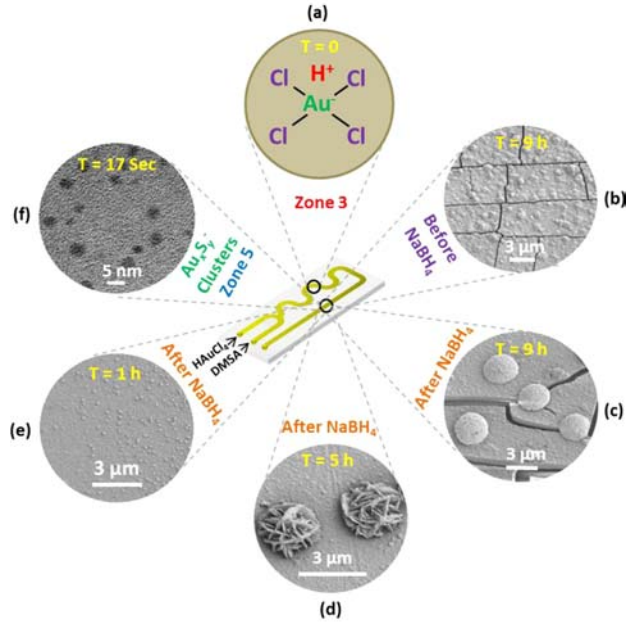

Figure 3. Schematic showing the different stages of spatially (and time) resolved growth process of gold nanostructures within the millifluidic chip.

representative of zones 1−4 (in Figure 1a), where the gold salt solution $HAuCl_4$ remained as it is, as shown by the XAS spectra taken at these zones (Figure 1d). TEM analysis also did not show formation of any particles at these zones 1−4. At ∼17 s, the first changes in the reduction process were noticed at zone 5 through XAS analysis (Figure 1d) as well as TEM imaging (Figure 3f), indicating the formation of $Au_xS_y^-$ nanoclusters. Therefore, the time-resolved growth was monitored at this zone. After an hour, the initial $Au_xS_y^-$ nanoclusters further increased in size to ∼300 nm (Figures 3e, 2a, and 1f). After a time interval of 5h, the formation of ∼3 μm in diameter gold structures that had corrugated petal-like nanostructured features can be noticed (Figures 3d, 2b). When the time of flow was increased to 9 h, one could notice that these structures further transformed into micro-hemispherical structures (Figures 3c, 2c). The Figure 3b indicated that the structural features remained same before and after the treatment with $NaBH_4$, and only the chemical nature changed from predominantly gold sulfide structures to metallic gold structures (Figure 1f). It is to be noted that all these different structures were formed in the center of the channel as the reaction was taking place at the interface of the flows from two inlets (based on X-ray tomography experiments as explained below and shown in Figure 4).

In order to understand the electronic and geometric properties of the gold structures formed at 9 h flow-time, the chip was dissected to obtain samples for XAS analysis. The XANES spectrum of the dissected samples showed formation

dx.doi.org/10.1021/ja400434c | J. Am. Chem. Soc. 2013, 135, 5450−5456

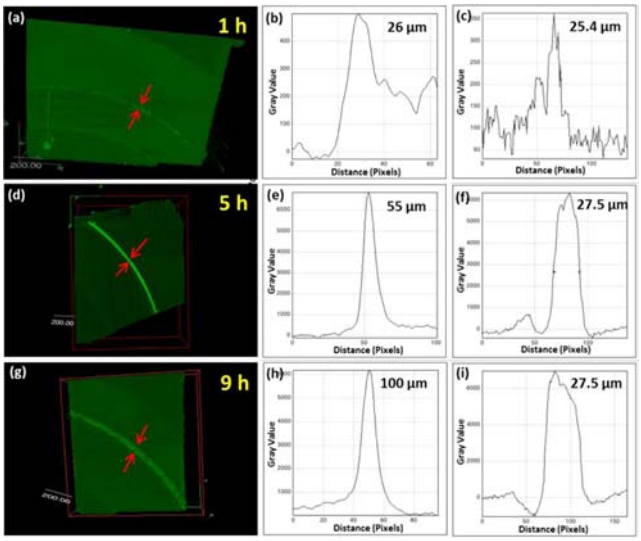

Figure 4. (a,d,g) 3-D X-ray tomographic images of the gold formed (marked by arrows) within the millifluidic channels after 1, 5, and 9 h flow-time; (b,e,h) width profile; and (c,f,i) thickness profile.

of metallic gold with Au−Au bonding without the need for $NaBH_4$ as a reducing agent. Calculations based on linear combination fitting using gold foil and gold sulfide reference compounds revealed 50% Au−S and 50% Au−Au bonding for this sample. There was a gradual increase in thickness of the $Au_xS_y^-$ growth observed within the millifluidic channels with increased flow-time of the precursors. Upon reduction with $NaBH_4$ for 15 min, the XANES linear combination fitting showed 17% Au−S and 83% Au−Au bonding, indicating reduction from Au(I) to Au(0). It is interesting to note that nearly 100% Au−Au bonding (corresponding to metallic gold) was observed only after performing catalysis (where the reducing agent $NaBH_4$ was utilized) over the resultant gold/gold sulfide nanostructures (Figure S9).

In addition to the morphological changes at different flow-times, we also observed dimensional changes of the nanostructured gold coating within the channel. After 9 h of flow-time, a thin yellow-colored deposit of ∼100 μm in width appeared at the center of the bottom surface of the millifluidic channel, *i.e.*, at the bottom of the interface of the two precursor solutions (Figure 4). This deposition primarily consisted of $Au_xS_y^-$ nanoclusters formed by the reaction of the two precursor solutions. After $NaBH_4$ flow was initiated, in order to reduce these structures to metallic gold, the color changed to black, corresponding to the reduction of the sulfide to metallic gold (Figure S10). Such a precise positioning of the gold coating within the channel was attributed to reaction occurring at the interface of the solutions due to the laminar flow within the channel. The black line, formed due to the reduction of Au (I) to Au (0) (Figure 4), contained gold nanostructures as described above. The EDAX elemental analysis confirmed that the black structures contained predominantly gold and traces of sulfur (Figure S11). Further, the width and thickness of the gold coating formed varied with the flow-time. In order to understand the time-resolved dimensional change of the coating, synchrotron radiation-based X-ray tomography was utilized.[31] Figure 4 shows the 3-D X-ray tomography images of the central gold coating obtained at 1, 5, and 9 h flow-time, respectively. The measured width and depth profiles (Figure 4) increased gradually with the flow-ime. Interestingly, the thickness of the film with deposited gold structures stopped at 27.5 μm even though its width gradually increased up to 100 μm with increasing flow-time.

The catalytic activity of nanostructured gold continues to be explored ever since the first report by Haruta *et al.*[32] While a majority of the catalysis applications of gold were focused on isolated gold nanoparticles supported through impregnation process,[33,34] there are very few reports regarding the catalytic activity of gold nanoparticles embedded within continuous flow microreactors.[15,35−37] We therefore, investigated the catalytic activity of the gold nanostructures formed within the millifluidic chip using the reduction of 4-nitrophenol (4-NP) to 4-aminophenol (4-AP)[38] as an example (Scheme 1).

Scheme 1. Reduction Reaction of 4-NP to 4-AP

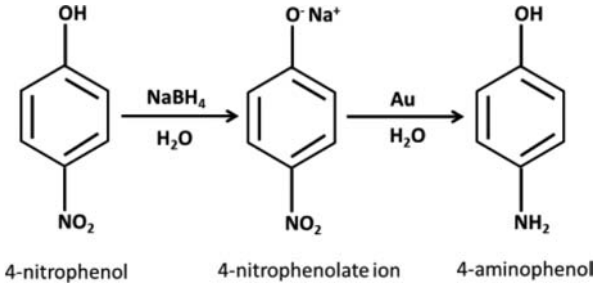

Initially, 4-NP was mixed with $NaBH_4$ to form its more reactive 4-nitrophenolate ion (4-NPI) form, which was later introduced into the chip at a flow-rate of 5 mL/h. It was converted into 4-AP, catalyzed by the deposited gold nanostructures. Figure 5a shows the UV−vis spectra of the standard solutions of 4-NP, 4-NPI, and 4-AP. The absorption spectrum of 4-NP with a λ_{max} of 316 nm was shifted to 399 nm indicating the formation of 4-NPI on mixing with $NaBH_4$. The 4-NPI was further converted to 4-AP (λ_{max} of 301 nm) by flowing it through the millifluidic channel containing the nanostructured gold deposited at the center. In the absence of the gold catalyst, conversion of 4-NPI was 20%; whereas in the presence of gold catalyst (formed at 9 h deposition time), there was 90.5% conversion of the 4-NPI (Figure 5b). The gold catalyst was also found to be catalytically active even after 80 h of continuous flow reaction. In order to understand the influence of flow-rate on catalysis, we carried out the catalysis at four different flow-rates (5, 20, 40, and 60 mL/h) and monitored the conversion of phenolate ion at these flow-rates. As shown in Figure S12, the highest conversion was found to take place at the lowest flow-rate of 5 mL/h. This is not surprising as one can expect better contact with the catalyst at lower flow-rate where the residence time is higher. The deposited nanostructured gold catalysts were also found to be active for conversion of ferricyanide to ferrocyanide (Figure S13). Here again, the gold catalyst (formed at 9 h flow-rate) had shown 85.5% conversion of the ferricyanide compared to 12% with no catalyst (Table 2).

■ CONCLUSIONS

In summary, we have demonstrated the use of a millifluidic chip for time-resolved mapping of the growth of gold nanostructures from solution using *in situ* XAS. The approach is novel and simple. It can be used to map the growth of a number of metallic nanostructures. Even though we demonstrated a time resolution of ∼5 ms, the tool developed has the potential to

dx.doi.org/10.1021/ja400434c | *J. Am. Chem. Soc.* 2013, 135, 5450−5456

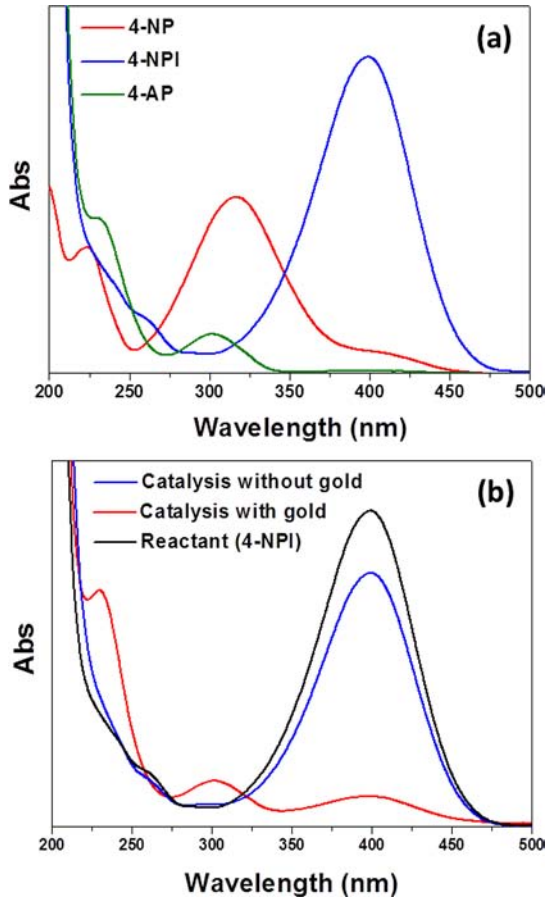

Figure 5. UV−vis spectra of (a) 4-NP, 4-NPI, and 4-AP. (b) Conversion of 4-NPI to 4-AP in a millifluidic chip reactor with and without gold.

provide nanosecond time resolution for *in situ* analysis of reactions in general and nanoparticle formation in particular by manipulating the flow-rates and size of the X-ray beam utilized for probing. In addition to synchrotron radiation-based *in situ* XAS probe, the tool 'in principle' can be combined with other spectroscopy probes such as UV−vis spectroscopy, Raman spectroscopy, SAXS, and so on.[39,40] Finally, this tool can also be utilized to obtain dimension and morphology controlled catalytic surfaces within the channels, and therefore it can be an excellent tool for continuous flow catalysis. In terms of versatility, it can be used to carryout and investigate the mechanistic aspects of a vast number of catalytic reactions. We envisage the utility of the tool not only to investigate the time-resolved formation of catalytically active structures but also for probing the catalysis in an operando mode with similar time resolutions. With the option to dissect the chips, one can envisage carrying out fundamental, atomically precise electronic and geometric investigations of metal clusters grown at different time intervals.[41] While the traditional field of microfluidics has not yet become widely used even after two decades of investigations, simple and easily accessible millifluidic-based tools as the one described here can revolutionize the ubiquity of lab-on-a-chip devices for high-value applications ranging from pharmaceuticals to micro-analytical tools.

■ ASSOCIATED CONTENT

Supporting Information

Experimental details and additional figures. This material is available free of charge via the Internet at http://pubs.acs.org.

■ AUTHOR INFORMATION

Corresponding Author

ckumar1@lsu.edu

Notes

The authors declare the following competing financial interest(s): One of the authors, Challa S. S. R. Kumar, is the founder of the company, Millifluidica, LLC (www.millifluidica.com), that is commercializing millifluidics-based technologies.

■ ACKNOWLEDGMENTS

This research work is supported as part of the Center for Atomic Level Catalyst Design, an Energy Frontier Research Center funded by the U.S. Department of Energy, Office of Science, Office of Basic Energy Sciences under award number DE-SC0001058 and also supported by Board of Regents under grants award number LEQSF (2009-14)-EFRC-MATCH and LEDSF-EPS(2012)-OPT-IN-15. MRCAT operations are supported by the Department of Energy and the MRCAT member institutions. The use of the Advanced Photon Source at ANL is supported by the U.S. Department of Energy, Office of Science, Office of Basic Energy Sciences, under contract no. DE-AC02-06CH11357. Financial support for JTM was provided as part of the Institute for Atom-efficient Chemical Transformations (IACT), an Energy Frontier Research Center funded by the U.S. Department of Energy, Office of Science, Office of Basic Energy Sciences.

■ REFERENCES

(1) Ade, H.; Zhang, X.; Cameron, S.; Costello, C.; Kirz, J.; Williams, S. *Science* **1992**, *258*, 972−975.
(2) Thornton, G. *Science* **2003**, *300*, 1378−1379.
(3) Sarma, L. S.; Chou, H. L.; Cheng, M. Y.; Taufany, F.; Lai, F. J.; Tsai, M. C.; Chang, S. H.; Hwang, B. J. In *Nanomaterials for the Life Sciences*, Wiley-VCH: Weinheim, Germany, 2008; Vol. 3, pp 377−409.
(4) Sun, Y. *Mater. Today* **2012**, *15*, 140−147.
(5) Whitesides, G. M. *Nature* **2006**, *442*, 368−373.
(6) deMello, A. J. *Nature* **2006**, *442*, 394−402.
(7) Zinoveva, S.; De Silva, R.; Louis, R. D.; Datta, P.; Kumar, C. S. S. R.; Goettert, J.; Hormes, J. *Nucl. Instrum. Methods Phys. Res., Sect. A* **2007**, *582*, 239−241.

Table 2. Summary of Catalysis Results

reaction	concentration of reactant (mol)	concentration of reductant (mol)	temperature (K)	flow-rate (ml/h)	conversion percentage of reactant (%)	
					with gold catalyst (9 h deposited chip)	without gold catalyst
reduction of 4-nitrophenol to 4-aminophenol	9×10^{-5}	0.65	298	5	90.5	20
reduction of ferricyanide to ferrocyanide	8.33×10^{-4}	0.01	298	5	85.5	12.2

dx.doi.org/10.1021/ja400434c | *J. Am. Chem. Soc.* 2013, 135, 5450−5456

(8) Wang, J. T.; Wang, J.; Han, J. J. *Small* **2011**, *7*, 1728−1754.
(9) Song, Y.; Modrow, H.; Henry, L. L.; Saw, C. K.; Doomes, E. E.; Palshin, V.; Hormes, J.; Kumar, C. S. S. R. *Chem. Mater.* **2006**, *18*, 2817−2827.
(10) Valencia, P. M.; Farokhzad, O. C.; Karnik, R.; Langer, R. *Nature Nanotechnol.* **2012**, *7*, 623−629.
(11) Oyanagi, H.; Sun, Z. H.; Jiang, Y.; Uehara, M.; Nakamura, H.; Yamashita, K.; Zhang, L.; Lee, C.; Fukano, A.; Maeda, H. *J. Synchrotron Rad.* **2011**, *18*, 272−279.
(12) Lorber, N.; Sarrazin, F.; Guillot, P.; Panizza, P.; Colin, A.; Pavageau, B.; Hany, C.; Maestro, P.; Marre, S.; Delclos, T.; Aymonier, C.; Subra, P.; Prat, L.; Gourdon, C.; Mignard, E. *Lab Chip* **2011**, *11*, 779−787.
(13) Biswas, S.; Miller, J. T.; Li, Y.; Nandakumar, K.; Kumar, C. S. S. R. *Small* **2012**, *8*, 688−698.
(14) Li, Y.; Sanampudi, A.; Reddy, V. R.; Biswas, S.; Nandakumar, K.; Yemane, D.; Kumar, C. S. S. R. *ChemPhysChem* **2012**, *13*, 177−182.
(15) Abahmane, L.; Knauer, A.; Köhler, J. M.; Groß, G. A. *Chem. Eng. J.* **2011**, *167*, 519−526.
(16) Gaur, S.; Miller, J. T.; Stellwagen, D.; Sanampudi, A.; Kumar, C. S. S. R.; Spivey, J. J. *Phys. Chem. Chem. Phys.* **2012**, *14*, 1627−1634.
(17) Nie, X.; Qian, H.; Ge, Q.; Xu, H.; Jin, R. *ACS Nano* **2012**, *6*, 6014−6022.
(18) Jin, R. *Nanotechnol. Rev.* **2012**, *1*, 31−56.
(19) Chen, S. P.; Yu, X. D.; Xu, J. J.; Chen, H. Y. *Biosens. Bioelectron.* **2011**, *26*, 4779−4784.
(20) Liang, R. P.; Meng, X. Y.; Liu, C. M.; Qiu, J. D. *Electrophoresis* **2011**, *32*, 3331−3340.
(21) Luo, C.; Fu, Q.; Li, H.; Xu, L.; Sun, M.; Ouyang, Q.; Chen, Y.; Ji, H. *Lab Chip.* **2005**, *5*, 726−729.
(22) Duan, G.; Cai, W.; Luo, Y.; Li, Z.; Li, Y. *Appl. Phys. Lett.* **2006**, *89*, 211905.
(23) Xia, Y.; Xiao, H. *J. Mol. Catal. A: Chem.* **2010**, *331*, 35−39.
(24) Wang, Z.; Zhang, J.; Ekman, J. M.; Kenis, P. J. A.; Lu, Y. *Nano Lett.* **2010**, *10*, 1886−1891.
(25) Wang, L.; Guo, S.; Hu, X.; Dong, S. *Electrochem. Commun.* **2008**, *10*, 95−99.
(26) Jiang, D.; Walter, M.; Dai, S. *Chem.—Eur. J.* **2010**, *16*, 4999−5003.
(27) Negishi, Y.; Tsukuda, T. *J. Am. Chem. Soc.* **2003**, *125*, 4046−4047.
(28) Chan, E. M.; Marcus, M. A.; Fakra, S.; ElNaggar, M.; Mathies, R. A.; Alivisatos, A. P. *J. Phys. Chem. A* **2007**, *111*, 12210−12215.
(29) Shan, C.; Han, D.; Song, J.; Ivaska, A.; Niu, L. *J. Mater. Res.* **2010**, *25*, 1755−1760.
(30) Li, H.; Wu, N. *Nanotechnology* **2008**, *19*, 275301.
(31) Prieto, G.; Zecevic, J.; Friedrich, H.; de Jong, K. P.; de Jongh, P. E. *Nat. Mater.* **2013**, *12*, 34−39.
(32) Haruta, M.; Kobayashi, T.; Sano, H.; Yamada, N. *Chem. Lett.* **1987**, *16*, 405−408.
(33) Valden, M.; Lai, X.; Goodman, D. W. *Science* **1998**, *281*, 1647−1650.
(34) Hughes, M. D.; Xu, Y. J.; Jenkins, P.; McMorn, P.; Landon, P.; Enache, D. I.; Carley, A. F.; Attard, G. A.; Hutchings, G. J.; King, F.; Stitt, E. H.; Johnston, P.; Griffin, K.; Kiely, C. J. *Nature* **2005**, *437*, 1132−1135.
(35) Adleman, J. R.; Boyd, D. A.; Goodwin, D. G.; Psaltis, D. *Nano Lett.* **2009**, *9*, 4417−4423.
(36) Wang, N.; Matsumoto, T.; Ueno, M.; Miyamura, H.; Kobayashi, S. *Angew. Chem.* **2009**, *121*, 4838−4840.
(37) Jamal, F.; Sebastien, G. J.; Mael, P.; Edmond, P.; Christian, R. *Microsyst. Technol.* **2012**, *18*, 151−158.
(38) Kuroda, K.; Ishida, T.; Haruta, M. *J. Mol. Catal. A: Chem.* **2009**, *298*, 7−11.
(39) Merlin, A.; Angly, J.; Daubersies, L.; Madeira, C.; Schöder, S.; Leng, J.; Salmon, J. B. *Eur. Phys. J. E: Soft Matter Biol. Phys.* **2011**, *34*, 58.
(40) Polte, J.; Erler, R.; Thünemann, A. F.; Sokolov, S.; Ahner, T. T.; Rademann, K.; Emmerling, F.; Kraehnert, R. *ACS Nano* **2010**, *4*, 1076−1082.
(41) Losovyj, Y. B.; Li, S. C.; Lozova, N.; Katsiev, K.; Stellwagen, D.; Diebold, U.; Kong, L.; Kumar, C. S. S. R. *J. Phys. Chem. C* **2012**, *116*, 5857−5861.